Experimental evaluation of plastic wake on growing fatigue cracks from the analysis of residual displacement fields

J.M. Vasco-Olmo[1*], F.A. Díaz[1], A. Camacho-Reyes[1], M.N. James[2, 3], F.V. Antunes[4]

[1] Departamento de Ingeniería Mecánica y Minera, University of Jaén, Jaén, Spain.
[2] School of Engineering, Computing and Mathematics, University of Plymouth, Plymouth, United Kingdom.
[3] Department of Mechanical Engineering, Nelson Mandela Metropolitan University, Port Elisabeth, South Africa.
[4] University of Coimbra, Centre for Mechanical Engineering, Materials and Processes (CEMMPRE), Department of Mechanical Engineering, Coimbra, Portugal.
[*]Corresponding author: jvasco@ujaen.es

Abstract. A growing fatigue crack gives rise to a plastically deformed wake of material that envelops the crack. In this work the plastic wake extent during fatigue crack growth is experimentally quantified by analysing the crack tip displacement fields measured with digital image correlation. A novel technique based on use of a yield criterion is proposed that uses the undamaged state of the specimen as the reference state in the image processing. The plastic wake was identified by differentiation of the residual displacement fields obtained with a near-zero load level to avoid any rigid body motion. The plastic wake extent was then found by assuming that the boundary between the elastic and plastic regions would occur when the equivalent stress was higher than the yield stress of the material. The results presented can contribute to a better understanding of the mechanisms driving fatigue crack propagation.

Keywords. Plastic wake, fatigue crack growth, residual displacement fields, digital image correlation, yield criterion.

Nomenclature:

a:	crack length
A:	plastic wake area
CT:	compact tension specimen
DIC:	digital image correlation
E:	Young's modulus
G:	shear modulus
N:	number of cycles
R:	ratio between the minimum and the maximum applied load
u, *v*:	horizontal and vertical components of the displacement field
UTS:	ultimate tensile strength
W:	width of the specimen
x, *y*:	Cartesian coordinates
ε_f:	fracture strain
ε_{xx}, ε_{yy}, ε_{xy}:	Cartesian components of the strain field
v:	Poisson's ratio
σ_{eq}:	equivalent stress
σ_{xx}, σ_{yy}, σ_{xy}:	Cartesian components of the stress field
σ_{ys}:	yield stress

1. Introduction

During fatigue crack growth under constant amplitude loading, a cyclic plastic zone is generated at the crack tip and a region of residual tensile deformation is left along the crack surfaces as the crack propagates. This plastically deformed region, known as the plastic wake, shields the crack from the full influence of the elastic stress field that drives fatigue crack growth and induces a reduction in crack opening displacement. These effects give rise to premature contact occurring between the crack flanks during unloading[1]. This premature contact mechanism is known as plasticity-induced crack closure. It was first observed by Elber in early 70's[2,3] and is a direct consequence of the plastic wake generated during fatigue crack growth. Experiments by Elber demonstrated that crack propagation rates are influenced not only by the conditions ahead of the crack tip, but also by the nature (magnitude and position) of the contact between the crack flanks behind the tip.

Subsequent research showed that there are other mechanisms that can lead to premature contact between the crack surfaces: these include roughness-induced crack closure[4–6], oxide-induced crack closure[7,8], viscous fluid-induced crack closure[9] and phase transformation-induced crack closure[10]. Nonetheless, plasticity-induced crack closure is the most widespread and extensively investigated fatigue crack shielding mechanism. More recent work has proposed that plastic shielding of the crack tip includes influences from a compatibility-induced interfacial shear stress at the elastic-plastic boundary as well as the effect of crack flank contact[11]. The plastic deformation attendant on fatigue crack propagation generates a residual stress field whose components depend on the applied load history[12], and this residual stress field also varies with load amplitude. Quantifying the residual stresses generated by a fatigue crack could therefore shed light on the relative contribution from parameters that influence fatigue crack propagation, such as the crack shielding effect, the applied load history or the stress ratio, among others. However, the study of the influence and effects of residual stresses in the plastic enclave that surrounds a fatigue crack is clearly a complex problem. This difficulty associated with experimental characterisation of the plastic wake is demonstrated by the fact that, to the authors' knowledge, there is virtually no reported work on the topic.

Doubts remain regarding how best to estimate the residual stresses left around a fatigue crack.

The effect of the residual stresses on fatigue crack propagation and their relaxation during fatigue cycling has, however, been investigated by a number of authors through analytical evaluation[13–15] and numerical studies[16–18]. These works concluded that residual stresses have a significant effect on fatigue crack propagation behaviour and that aspects such as the applied load history and the stress ratio have a significant influence on the residual stress field. Therefore, a detailed description of the residual stress field must include any wake contact stresses and those generated by compatibility requirements at the boundary between the elastic and plastic regions in the specimen. These arise because Poisson's ratio is different in the two regions, as plastic deformation is a constant volume process. Such an approach is clearly more complex than simply considering a detailed description of the cyclic plastic deformation in front of the crack tip, which is, in itself, very difficult[12].

There are various methods or techniques that can be used to measure residual stresses[Error! Reference source not found.]. They are commonly grouped as destructive, semi-destructive and non-destructive techniques. The most usual destructive and semi-destructive techniques are incremental hole-drilling[20] and the ring core technique[21]. Amongst the non-destructive methods, some of the most useful 3D techniques are synchrotron X-ray diffraction[22–24], neutron diffraction[25,26] and the ultrasonic methods. Although some work has been published that has used synchrotron diffraction to measure crack tip residual stress fields and explore the possibility of crack wake contact e.g.[24,27,28], insufficient beam time is generally available in such experiments to quantify, in the required detail, the residual stress field or plasticity-induced wake contact. Nonetheless, a significant body of work has been published that used X-ray and neutron diffraction to identify crack-tip deformation fields and residual stresses. Examples include the work by Korsunsky at el.[29] who presented an overview of experimental and modelling studies of fatigue crack growth rates in Ti-6Al-4V alloy, Coules et al.[30] who used neutron diffraction to obtain full-field strain measurements and linked this with finite element analysis to demonstrate that the effect of residual stresses on the crack growth resistance curve in 7475-T751 alloy could be understood using elastic-plastic fracture mechanics, and

Salvati et al.[31] who studied the changes in fatigue crack propagation following a single compressive underload using synchrotron X-ray diffraction and DIC. Besides the above techniques, other localised techniques capable to evaluate residual stress are high-resolution electron back scatter diffraction (HR-EBSD), focused ion beam-digital image correlation (FIB-DIC)[32] or nano-scale focused synchroton XRD[33].

Nowadays, digital image correlation (DIC) is a well-established optical technique used in research on fracture mechanics and fatigue crack propagation. It allows crack tip displacement fields to be measured with high resolution and accuracy[34]. DIC has been previously used successfully by some the authors of the current work in such areas as the estimation of stress intensity factors (SIFs)[35], evaluation of fatigue crack shielding and the effect of overloads on fatigue crack growth[36,37], characterisation of the fatigue crack growth rates[38], quantification of the size and shape of crack tip plastic zone[39] or measurement of crack tip opening displacement (CTOD) as a characterising parameter for fatigue crack propagation[40].

In the present work DIC was applied to measuring residual displacement fields for fatigue cracks subject to constant amplitude loading in order to quantify the plastic wake left behind the crack tip. Residual displacements were measured using a novel method that considered the undamaged state of the specimen as the reference state in the image processing. To the author's knowledge, this is the first time that DIC has been used in this way to obtain the residual displacement fields in a fracture problem. The undamaged state image is then correlated with other images acquired at a load level close to zero, for various crack length values. This avoids including any extraneous rigid body motion in the analysis. In addition, the use of the undamaged state of the specimen allows identification of the accumulated damage during fatigue crack propagation. The effects of the applied load history or load changes during fatigue cycling on fatigue crack growth rates can be deduced from the analysis of the residual displacement fields, which can potentially contribute to an improved understanding of the mechanisms driving fatigue crack propagation.

The technique for identifying the plastic wake applies a yield criterion to the stress fields that are obtained from the strain fields estimated by differentiating the residual displacement fields measured via DIC. The plastic wake extent is

identified as that region where the equivalent stress is higher than the yield stress of the material.

2. Experimental work

Two compact tension (CT) specimens (Figure 1a) were manufactured from a sheet of commercially pure Grade 2 titanium with a thickness of 1 mm and tested under constant amplitude fatigue with a maximum load of 750 N at stress ratio values of 0.1 and 0.6. The equivalent values of stress intensity factor at maximum load are 19 MPa·m$^{1/2}$ and 47 MPa·m$^{1/2}$, corresponding with crack lengths of 3 mm and 9.5 mm, respectively. These crack lengths represent the notch and the longest crack studied, where SIF values are approaching the fracture toughness of the material. The chemical composition for Grade 2 titanium is given in Table 1 and the tensile data are provided in Table 2.

Both sides of the two specimens were prepared so as to allow simultaneous measurements of the displacement fields by DIC on one side and crack length on the other. The side used for DIC was sprayed with a random black speckle pattern over a white background (Figure 1b), while the other side of the specimens was ground and polished to allow tracking of the crack tip position with a macro-zoom lens (MLH-10X EO).

An Instron Electropuls E3000 electrodynamic machine was used for fatigue testing at a frequency of 10 Hz. A CCD camera, fitted with a macro-zoom lens similar to the one used to track crack tip position, gave increased spatial resolution in the region surrounding the crack tip, and was positioned perpendicularly to the side of the specimens. Fatigue cycling was periodically paused to allow data acquisition at different crack lengths and to obtain an image at near-zero loads.

The CCD camera used to view the speckled surface was set up to give a field of view of 17.3 x 13 mm (a resolution of 13.7 µm/pixel) with the crack path located at the centre of the image. A fibre optic ring light was placed around the zoom lens to illuminate the specimen surface and in this way capture higher quality images.

3. Experimental quantification of plastic wake

As noted above, the technique presented in this work is based on applying a yield criterion to the residual displacement data that fatigue crack growth leaves

in its wake. Although 2D-DIC was used in this work, any technique that allows displacement fields to be obtained would be applicable. The sequential procedure is described in the following paragraphs.

In the first step the residual displacement fields that remain around the crack tip at near-zero load are measured, and these incorporate effects of both the applied loads and those induced by plasticity as a consequence of crack propagation. Measuring the displacement fields at a near-zero load level avoids incorporating into the subsequent analysis any rigid body motion that might have arisen during the loading half cycle. In this work 10 N was the load level used to define the unloaded state of the specimen since it was the lowest load could be reliably applied with the load cell on the testing machine and represents only 1.3% of the maximum load in the fatigue cycle. A particularly innovative aspect of this work is that residual displacement fields at each crack length were obtained by comparison with the unloaded state that was analysed using the undamaged state of the specimen as a reference. Figure 2 shows an example of the horizontal and vertical residual displacement maps obtained with a crack 9.2 mm long tested at $R = 0.6$.

In the second step, the strain fields at the crack tip are determined by differentiation of the residual displacement fields using the Green-Lagrange strain tensor (pages 88–91 of Mechanics of Solids book[41]) because it considers second order terms and is hence more accurate than expressions that use only first order terms. This strain tensor is given as follows:

$$
\begin{pmatrix} \varepsilon_{xx} \\ \varepsilon_{yy} \\ \varepsilon_{xy} \end{pmatrix} = \begin{pmatrix} \dfrac{\partial u}{\partial x} \\ \dfrac{\partial v}{\partial y} \\ \dfrac{\partial u}{\partial y} + \dfrac{\partial v}{\partial x} \end{pmatrix} + \frac{1}{2} \begin{pmatrix} \dfrac{\partial u}{\partial x} & 0 & \dfrac{\partial v}{\partial y} & 0 \\ 0 & \dfrac{\partial u}{\partial y} & 0 & \dfrac{\partial v}{\partial y} \\ \dfrac{\partial u}{\partial y} & \dfrac{\partial u}{\partial x} & \dfrac{\partial v}{\partial y} & \dfrac{\partial v}{\partial x} \end{pmatrix} \begin{pmatrix} \dfrac{\partial u}{\partial x} \\ \dfrac{\partial u}{\partial y} \\ \dfrac{\partial v}{\partial x} \\ \dfrac{\partial v}{\partial y} \end{pmatrix} \tag{1}
$$

Therefore, the Green-Lagrange tensor includes the linear infinitesimal tensor for small strains (first term in equation 1) and the nonlinear terms for large strains (second term in equation 2).

Once the residual strains have been obtained, the residual stress fields can be calculated using Hooke's law:

$$\sigma_{xx} = \frac{E}{1-v^2}\left(\varepsilon_{xx} + v\varepsilon_{yy}\right)$$

$$\sigma_{yy} = \frac{E}{1-v^2}\left(\varepsilon_{yy} + v\varepsilon_{xx}\right) \qquad (2)$$

$$\sigma_{xy} = 2G\varepsilon_{xy}$$

Where $G = E/2(1+v)$ is the shear modulus, and E and v are the Young's modulus and the Poisson's ratio of the material, respectively.

The equivalent stress is then calculated by applying a suitable yield criterion. In this work the von Mises criterion was used as it has been shown to be the most appropriate for a ductile material[42,43]. A first order estimate of the size and shape of the plastic wake can then be obtained by connecting all points where the yield criterion is met, i.e. where the equivalent stress is higher than the yield stress of the material. Figure 3a shows this region in a binary black-white image, and this identifies the monotonic plastic wake generated during fatigue propagation that surrounds the crack. A greater than or equal operator (>=) was used to convert the equivalent stress map analysed to a binary black and white format. Thus, the yield stress of the material was used to the right operand to return true if the equivalent stress was greater or equal to the yield stress and false otherwise.

The current work considers the area of the plastic wake as a variable that contains useful information on crack growth, and the method clearly provides an efficient and powerful way for making quantitative measurements of the monotonic plastic wake region. Once this region has been identified, its area can be calculated using the function "bwarea", implemented in Matlab®. This function is used to estimate the area of objects in a black/white binary image. To use this function, the equivalent stress map analysed must be converted to a binary black-white format before the area of the plastic wake can be estimated. Figure 3b shows the plastic wake region isolated from the rest of the map and on a completely black background to assist in estimation of its area. The area of the plastic wake in this case of a 9.2 mm long crack grown at $R = 0.6$ is obtained as 13.51 mm^2.

4. Experimental results

The procedure described above was applied to all the data for the various crack lengths analysed and this allowed the evolution of the plastic wake to be

followed as the crack grew. Figure 4 shows a plot of crack length as a function of the number of cycles for the two specimens tested at stress ratio values of 0.1 and 0.6. In addition, Table 3 details the specific values of number of cycles and the crack length in both cases. Figure 5 shows plastic wake data corresponding to three different crack lengths for each of the two specimens. The figure shows data for crack lengths of 4.8 mm, 6.9 mm and 9.4 mm for the specimen tested at R = 0.1 and 4.7 mm, 6.9 mm and 9.2 mm for the specimen tested at R = 0.6. The area of the plastic wake obtained in each case is also given.

The plastic wake outline contour can also be found and plotted in a single figure to show the evolution of the plastic wake during fatigue crack propagation as shown in Figure 6. The contours shown for the specimen tested at R = 0.1 correspond to those cases of Table 3 between datapoints 1 (5000 cycles, 3.5 mm crack) and 23 (13500 cycles, 9.4 mm crack), while for the specimen tested at R = 0.6, the contours correspond to the cases between datapoints 5 (25000 cycles, 3.4 mm) and 25 (74000 cycles, 9.2 mm crack). A gradual increase of the plastic wake is observed as the crack propagates that agrees with the gradual development of plasticity, and consequently the residual stresses, in a growing fatigue crack at constant amplitude loading cycle. These results demonstrate that the plastic wake can be identified and calculated from the analysis of the residual displacement fields generated during fatigue crack growth using DIC. From a direct observation of the contours, it is difficult to establish any differences among them. For this reason, trying to find a possible effect of the stress ratio, the qualitative comparison in Figure 6 can be extended to provide quantitative data through estimating the area of the plastic wake. Figure 7 shows the variation in the plastic wake area with crack length, normalised by the specimen width, for both stress ratios. The trend in the data can be fitted with a quadratic polynomial (fit coefficient of 0.997 in the case of the specimen tested at R = 0.1 and 0.999 for the specimen tested at R = 0.6), giving the following expressions that relate the plastic wake area with the normalised crack length (a/W):

R = 0.1: $$A = 117.05\left(\frac{a}{W}\right)^2 - 35.73\frac{a}{W} + 3.1903 \qquad (3)$$

$$R = 0.6: \qquad\qquad A = 110.84\left(\frac{a}{W}\right)^2 - 25.108\,\frac{a}{W} + 1.301 \qquad\qquad (4)$$

To the knowledge of the authors, no similar mathematical fitting for other parameters used in quantifying damage based on crack tip plasticity have been published in the literature. There was little difference between the plastic wake area at either stress ratio for normalised crack lengths below 0.25. This is perhaps not surprising, as the maximum stress was the same in both tests and the influence of the stress ratio would be minimised when the plastic wake area is smaller at the shorter crack lengths. A divergence in the data occurs above a/W approximately ≥ 0.30. This is likely to reflect both the increased amount of reversed plasticity that will occur at $R = 0.1$ during the unloading half cycles and the higher mean stress in cycling at $R = 0.6$ that increases the ratcheting strain with continued cycling. This can be interpreted as leading to a smaller compressive residual stress zone in the specimen tested at $R = 0.6$ a higher residual tensile stress field along the crack path than would be the case for the specimen tested at low R-ratio. Hence, the larger compressive residual stress region in the case of the specimen tested at $R = 0.1$ would cause a greater retardation effect on fatigue crack growth than for a specimen tested at R-ratio of 0.6, i.e. a greater level of plasticity-induced crack tip shielding. This behaviour was reported in a previous work[39] where a retardation effect on fatigue propagation was observed in the case of the specimen tested at low R-ratio, but was not seen for a specimen tested at $R = 0.6$.

Figure 8 compares the trends in the maximum values of the residual vertical displacements (v) as a function of normalised crack length (a/W). It is observed that the values are higher in the test at $R = 0.6$ for $a/W ≥ 0.3$. Thereafter, the divergence gradually increases in the results obtained at the two stress ratios. This behaviour, observed in Figure 8, links well with that observed in the curves for plastic wake area given in Figure 7, and with the development of higher residual tensile stresses in the case of the specimen tested at the higher R-ratio.

The experimental method for obtaining crack wake area, as outlined in this paper, has been based on the uniaxial tensile yield stress and could be further refined through use of the cyclic stress-strain curve since the plastic wake is the

region plastically deformed left as a fatigue crack propagates. However, it is important to note that all discussion of results and conclusions drawn, especially on the comparison between the two stress ratios analysed, would not be affected.

These results support the conclusions drawn by other authors[16,18,44,45] that residual stresses can significantly affect fatigue crack propagation behaviour. It seems likely that studying the residual displacement fields could shed additional light on some of the effects of applied load history, or changes in the load amplitude, on fatigue crack growth rate. Further insights could also be gained on the crack wake contact phenomenon since it is, at least in part, a direct consequence of the plastic deformation left in the wake of a propagating crack[2]. Therefore, although the study of the residual displacement fields could contribute to a better understanding on the contact phenomenon between the crack flanks; further work must be performed on how the fields can be related with the shielding effect during fatigue crack propagation. Thus future work might explore the relationship between the plastic wake left by a growing fatigue crack and the shielding effect by using the stress intensity factors calculated from the analysis of the residual displacement fields. In this respect, the CJP model can be useful in characterising crack tip displacement fields due to its demonstrated ability to incorporate the shielding effects of the plastic enclave on a growing fatigue crack[11]. The discussions and conclusions drawn in this work can be extended through such additional work on investigating how the influences of shielding can be linked with the plastic wake left by a propagating fatigue crack. In addition, it is believed that the proposed methodology could be used to explore the effect of an overload on a growing fatigue crack, because the overload effect would be reflected in the residual displacement fields. Much work has been published dealing with overloads. Simpson et al.[46] provide a useful starting point on the topic.

5. Conclusions

In this paper a DIC-based method has been outlined that allows experimental determination of the plastic wake region that is generated by a growing fatigue crack. The area of the plastic wake has been used as a quantifying parameter for residual displacements in the wake. The experimental method was applied

on two CT titanium specimens, fatigued at stress ratios of 0.1 and 0.6. For both specimens, a quadratic relationship between the plastic wake area and the normalised crack length a/W was obtained. The plastic wake region was found by differentiating the residual displacement fields obtained for a near-zero load level so as to avoid any rigid body motion that might occur during loading. In this work, 10 N was used as the reference load that defined the unloaded state of the specimen; this represents 1.3% of the maximum applied load. A particularly innovative aspect of the work is the use of the undamaged state of the specimen as the reference for image processing. Applying the von Mises yield criterion then gives the plastic wake area as that region where the equivalent stress is higher than the yield stress of the material. Stress fields were then determined from the strain fields via Hooke's law.

This work has demonstrated that is experimentally possible to measure the residual displacement fields using DIC by taking the undamaged specimen state as the reference image and correlating this field with that obtained for the unloaded state at any particular crack length during fatigue crack propagation. This opens up the possibility that the influence of prior history or changes in load amplitude can be investigated from an analysis of the residual displacement field. The technique outlined in this paper therefore offers strong potential to contribute to a better understanding of the mechanisms driving fatigue crack growth and plasticity-induced shielding.

Author Contribution Statement

The original idea was conceived by F.A. Díaz and M.N. James and countersigned by F.V. Antunes. J.M. Vasco-Olmo and A. Camacho-Reyes performed the experimental work, composed by the fatigue tests, data collection and its processing to obtain the experimental results. All authors worked on the

analysis, interpretation and discussion of the results, where the most critical feedback was provided by F.A. Díaz, F.V. Antunes and M.N. James. J.M. Vasco-Olmo took the lead in writing the original version of the manuscript and the rest of authors contributed to its final version through their critical comments, editions and reviews. All authors agree on the order in which their names are listed in the manuscript.

Highlights:

- Quantification of the plastic wake by analysing residual displacement fields using DIC.
- Use of the undamaged state of the specimen as the reference for image processing.
- Plastic wake area as quantifying parameter for residual fatigue displacements.
- Application of the von Mises yield criterion to estimate the plastic wake extent.

References

1. Suresh S. *Fatigue of Materials*. UK: Cambridge University Press; 1998.
2. Elber W. Fatigue crack closure under cyclic tension. *Eng Fract Mech.* 1970; 2: 37–45.
3. Elber W. The significance of fatigue crack closure. In: Damage Tolerance in Aircraft Structures, M. Rosenfeld ed. *ASTM STP 486, American Society for Testing and Materials*. West Conshohocken, PA; 1971: 230–242.
4. Suresh S, Ritchie RO. A geometric model for fracture surface roughness-induced crack closure during fatigue crack-growth. *J. Met.* 1982; 34: 71.
5. Ritchie RO, Suresh S. Some considerations on fatigue crack closure at near-threshold stress intensities due to fracture surface morphology. *Metall Trans A.* 1982; 13: 937–940.
6. Suresh S, Ritchie RO. A geometric model for fatigue crack closure induced by fracture surface roughness. *Metall Trans A.* 1982, 13: 1627–1631.
7. Suresh S, White C, Ritchie RO. Oxide-induced crack closure. *J. Met.* 1980, 32: 76.
8. Suresh S, Zamiski GF, Ritchie RO. Oxide-induced crack closure: an explanation for near-threshold corrosion fatigue crack growth behaviour. *Metall Trans A.* 1981, 12: 1435–1443.

9. Endo K, Okada T, Hariya T. Fatigue crack propagation in bearing metals lining of steel plates in lubricating oil. *Bulletin of the JSME.* 1972, 15: 439–445.

10. Pineau AG, Pelloux RMN. Influence of strain-induced martensitic transformations on fatigue crack growth rates in stainless steels. *Metall Trans A.* 1974, 5: 1103–1112.

11. James MN, Christopher CJ, Lu Y, Patterson EA. Local crack plasticity and its influences on the global elastic stress field. *Int J Fatigue.* 2013, 46: 4–15.

12. Pippan R, Hohenwarter A. Fatigue crack closure: a review of the physical phenomena. *Fatigue Fract Eng Mater Struct.* 2017, 40: 471–495.

13. Lang M. A model for fatigue crack growth, part II: modelling. *Fatigue Fract Eng Mater Struct.* 2000, 23: 603–618.

14. Zhuang WZ, Halford GR. Investigation of residual stress relaxation under cyclic load. *Int J Fatigue.* 2001, 23: S31–S37.

15. Noroozi A, Glinka G, Lambert S. Prediction of fatigue crack growth under constant amplitude loading and a single overload based on elasto-plastic crack tip stresses and strains. *Eng Fract Mech.* 2008, 75: 188–206.

16. Fischer FD, Davies W, Pippan R, Pointner P. Some comments on surface cracks in rails. *Fatigue Fract Eng Mater Struct.* 2006, 29: 938–948.

17. González-Herrera A, Zapatero J. Numerical study of the effect of plastic wake on plasticity-induced crack closure. *Fatigue Fract Eng Mater Struct.* 2009, 32: 249–260.

18. Predan J, Pippan R, Gubeljak N. Fatigue crack propagation in threshold regime under residual stresses. *Int J Fatigue.* 2010, 32: 1050–1056.

19. Rossini, NS, Dassisti, M, Benyounis, KY, Olabi, AG. Methods of measuring residual stresses in components. *Mater Des.* 2012, 35: 572–588.

20. Niku-Lari A, Lu J, Flavenot JF. Measurement of residual-stress distribution by the incremental hole-drilling method. *J Mech Work Technol.* 1985, 11: 167–188.

21. Masláková K, Trebuňa F, Frankovský P, Binda M. Applications of the strain gauge for determination of residual stresses using ring-core method. *Procedia Eng.* 2012, 48: 396–401.

22. James MN, Hughes DJ, Hattingh DG, Bradley GR, Mills G, Webster PJ. Synchrotron diffraction measurement of residual stresses in friction stir

welded 5383-H321 aluminium butt joints and their modification by fatigue cycling. *Fatigue Fract Eng Mater Struct.* 2003, 27: 187–202.

23. James, MN, Newby M, Hattingh DG, Steuwer A. Shot peening of steam turbine blades: residual stresses and their modification by fatigue, *Procedia Eng.* 2010, 2: 441–451.

24. Salvati E, Zhang H, Fong KS, Song X, Korsunsky AM. Separating plasticity-induced closure and residual stress contributions to fatigue crack retardation following an overload. *J Mech Phys Solids.* 2017, 98: 222–235.

25. Allen AJ, Hutchings MT, Windsor CG, Andreani C. Neutron diffraction methods for the study of residual stress fields. *Adv Phys.* 1985, 34: 445–473.

26. James MN, Ting S-P, Bosi M, Lombard H, Hattingh DG. Residual strain and hardness as predictors of the fatigue ranking of steel welds, *Int J Fatigue.* 2009, 31: 1366–1377.

27. James MN, Hattingh DG, Hughes DJ, Wei L-W, Patterson EA, da Fonseca JQ, Synchrotron diffraction investigation of the distribution and influence of residual stresses in fatigue. *Fatigue Fract Eng Mater Struct.* 2004, 27: 609–622.

28. Thielen M, Schaefer F, Gruenewald P, Laub M, Marx M, Meixner M, Klaus M, Motz C. In situ synchrotron stress mappings to characterize overload effects in fatigue crack growth, *Int J Fatigue* 2019, 121: 155–162.

29. Korsunsky, A.M., Song, X., Belnoue, J., Jun, T., Hofmann, F., De Matos, P.F.P., Nowell, D., Dini, D., Aparicio-Blanco, O., Walsh, M.J. Crack tip deformation fields and fatigue crack growth rates in Ti-6Al-4V, *Int J Fatigue* 2009, 31(11): 1771–1779.

30. Coules, H.E., Horne, G.C.M., Abburi Venkata, K., Pirling, T. The effects of residual stress on elastic-plastic fracture propagation, *Mater Des.* 2018, 143: 131–140.

31. Salvati, E., Sui, T., Zhang, H., Lunt, A.G.J., Fong, K.S., Song, X., Korsunsky, A.M. Elucidating the mechanism of fatigue crack acceleration following the occurrence of an underload. *Adv Eng Mater.* 2016, 18(12): 2076–2087.

32. Salvati, E., O'Connor, S., Sui, T., Nowell, D., Korsunsky, A.M. A study of overload effect on fatigue crack propagation using EBSD, FIB-DIC and FEM methods. *Eng Fract Mech*. 2016, 167: 210–223.

33. Romano-Brandt, L., Salvati, E., Le Bourhis, E., Moxham, T., Dolbnya, I.P., Korsunsky, A.M. Nano-scale residual stress depth profiling in Cu/W nano-multilayers as a function of magnetron sputtering pressure. Surf Coat Technol. 2020, 381: https://doi.org/10.1016/j.surfcoat.2019.125142

34. Sutton MA, Orteu JJ, Schreier HW. *Image Correlation for Shape, Motion and Deformation Measurements: Basic Concepts, Theory and Applications*. USA: Springer Science+Business Media, LLC; 2009.

35. Du Y, Díaz FA, Burguete RL, Patterson EA. Evaluation using digital image correlation of stress intensity factors in an aerospace panel. *Exp Mech.* 2011, 51: 45–57.

36. Vasco-Olmo JM, Díaz FA, García-Collado A., Dorado R. Experimental evaluation of crack shielding during fatigue crack growth using digital image correlation. *Fatigue Fract Eng Mater Struct.* 2015, 38: 223–237.

37. Vasco-Olmo JM, Díaz FA. Experimental evaluation of the effect of overloads on fatigue crack growth by analysing crack tip displacement fields. *Eng Fract Mech.* 2016, 166: 82–96.

38. Yang B, Vasco-Olmo JM, Díaz FA, James MN. A more effective rationalisation of fatigue crack growth rate data for various specimen geometries and stress ratios using the CJP model. *Int J Fatigue* 2018, 114: 189–197.

39. Vasco-Olmo JM, James MN, Christopher CJ, Patterson EA, Díaz FA. Assessment of crack tip plastic zone size and shape and its influence on crack tip shielding. *Fatigue Fract Eng Mater Struct.* 2016, 39: 969–981.

40. Vasco-Olmo JM, Díaz FA, Antunes FV, James MN. Characterisation of fatigue crack growth using digital image correlation measurements of plastic CTOD. *Theor Appl Fract Mech.* 2019, 101: 223–341.

41. Singh, AK. *Mechanics of Solids*. India: Prentice-Hall of India; 2010.

42. Christensen, RM. How Do Mises and Tresca Fit In, Failure Theory for Materials Science and Engineering. Accessed on 03/11/2021. www.failurecriteria.com/misescriteriontr.html.

43. Taylor GI, Quinney H. The plastic distortion of metals. *Philosophical Transactions of the Royal Society of London. Series A, Containing Papers of a Mathematical or Physical Character* 1931, 230: 323–362.

44. Ritchie RO. Mechanisms of fatigue crack propagation in metals, ceramics and composites: role of crack tip shielding. *Mater Sci Eng A.* 1988, 16: 15–28.

45. Suresh S. Fatigue crack deflection and fracture surface contact: micromechanical models. *Metall Trans A.* 1985, 16: 249–260.

46. Quantifying fatigue overload retardation mechanisms by energy dispersive X-ray diffraction. *J. Mech. Phys. Solids.* 2019, 124: 392–410.

Tables

Table 1 Chemical composition for commercially pure titanium grade 2

Element (wt %)	N	C	H	Fe	O	Ti
Requirement	≤0.05	≤0.08	≤0.015	<0.20	≤0.20	Balance
Result	<0.01	0.01	0.002	0.10	0.12	Balance

Table 2 Measured mechanical properties

Parameter	E (GPa)	UTS (MPa)	σ_{ys} (MPa)	ε_f (%)	v
Value	105	448	390	20	0.33

Table 3 Data of number of cycles and crack lengths for both tests

|	$R = 0.6$			$R = 0.1$	
data	N (cycles)	a (mm)	data	N (cycles)	a (mm)
0	0	3.0	0	0	3.0
1	5000	3.0	1	5000	3.5
2	10000	3.0	2	7000	4.2
3	15000	3.1	3	7400	4.4
4	20000	3.2	4	7800	4.6
5	25000	3.4	5	8200	4.8
6	30000	3.6	6	8600	5.0
7	35000	3.8	7	9000	5.2
8	40000	4.1	8	9400	5.5
9	44000	4.4	9	9800	5.7
10	48000	4.7	10	10200	5.9
11	52000	5.1	11	10600	6.2
12	55500	5.4	12	11000	6.5
13	58500	5.8	13	11400	6.9
14	61000	6.1	14	11700	7.1
15	63000	6.4	15	11900	7.3
16	64500	6.7	16	12100	7.5
17	66000	6.9	17	12300	7.8
18	67500	7.3	18	12500	8.0
19	69000	7.6	19	12700	8.2
20	70000	7.9	20	12900	8.5
21	71000	8.1	21	13100	8.7
22	72000	8.5	22	13300	9.0
23	72750	8.7	23	13500	9.4
24	73500	9.0			
25	74000	9.2			

Figures
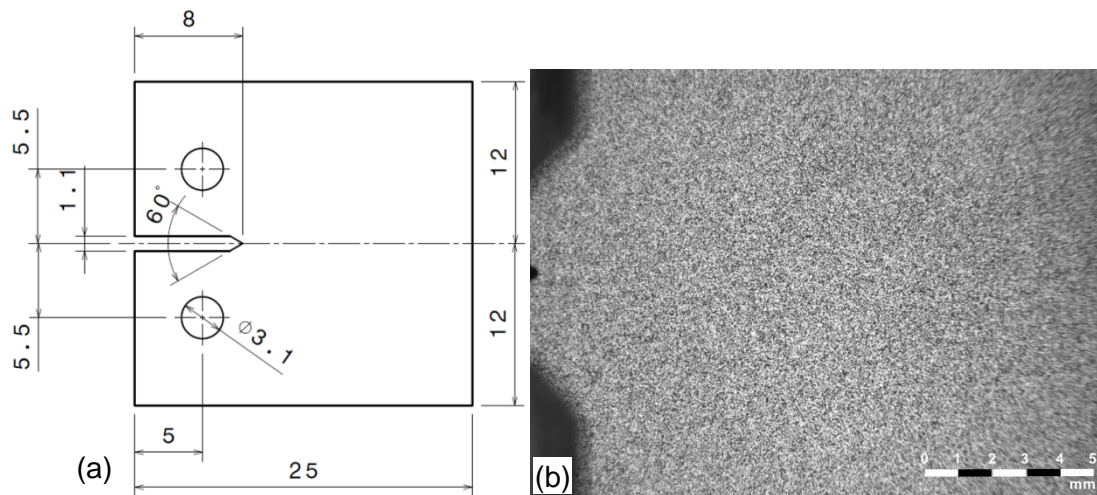
Figure 1   (a) Dimensions of the CT specimens (mm). (b) Illustration of the speckle pattern sprayed onto the specimen surface for making DIC measurements.
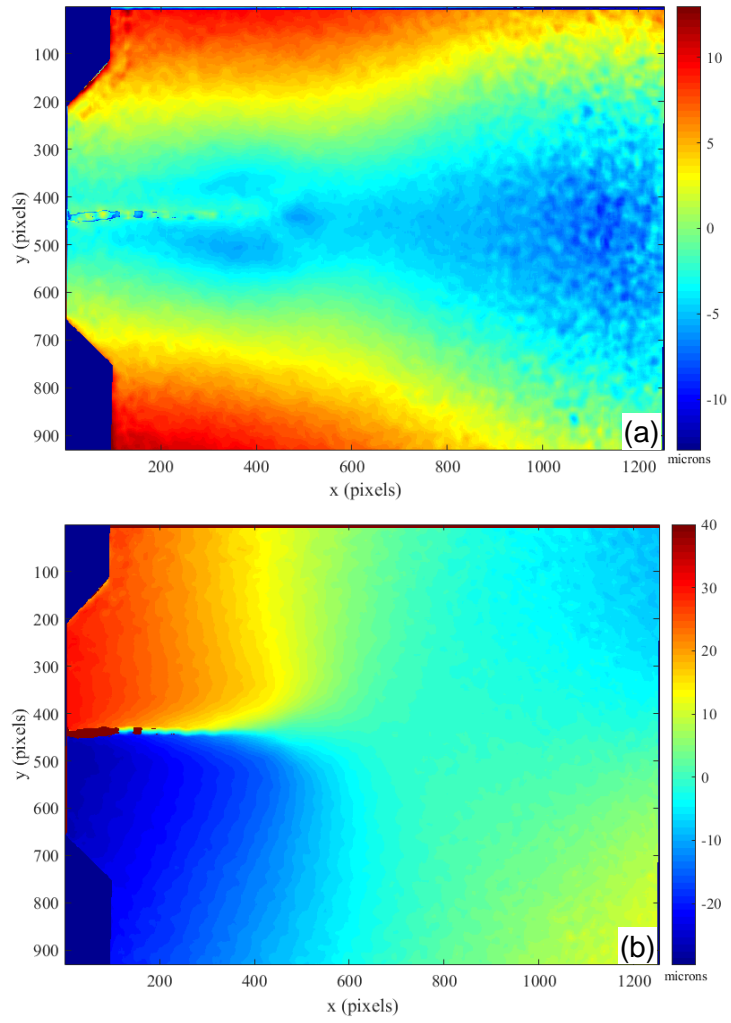
Figure 2   Residual displacement maps for a specimen tested at R = 0.6 and a crack length of 9.2 mm. (a) Horizontal and (b) Vertical
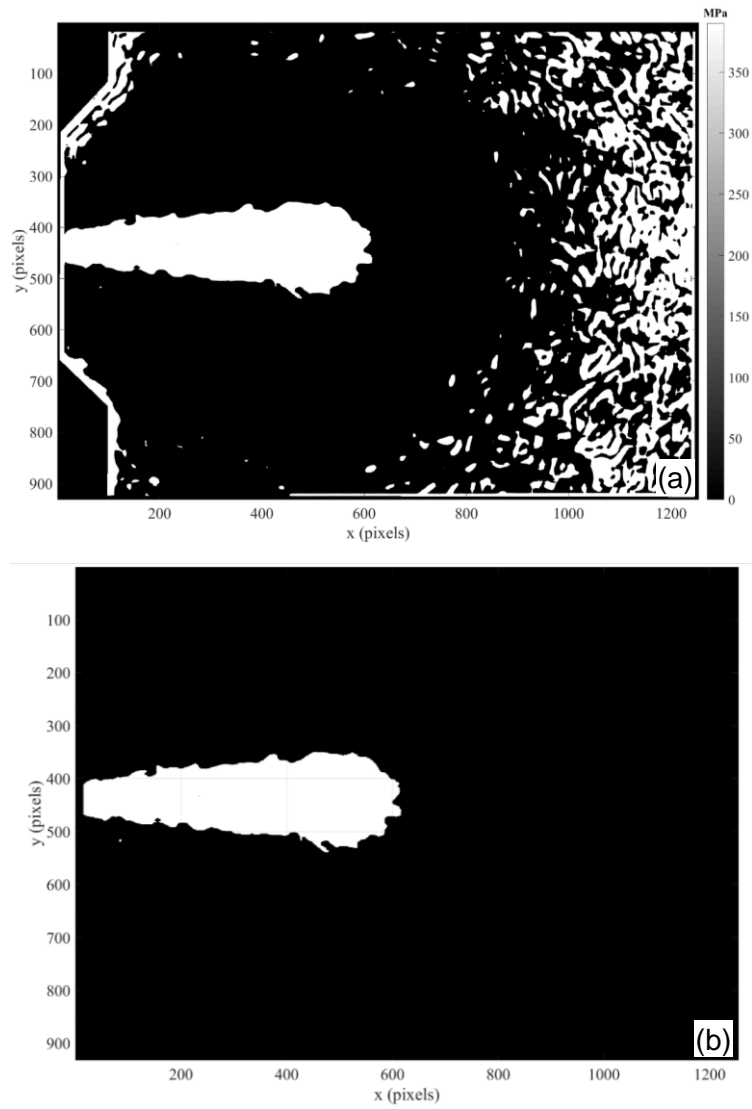
Figure 3   Illustrations showing (a) the equivalent stress map for the region where its value exceeds the yield stress for a crack 9.2 mm long tested at $R = 0.6$; (b) the extent of the plastic wake isolated from the rest of the stress map to assist in quantifying its area.
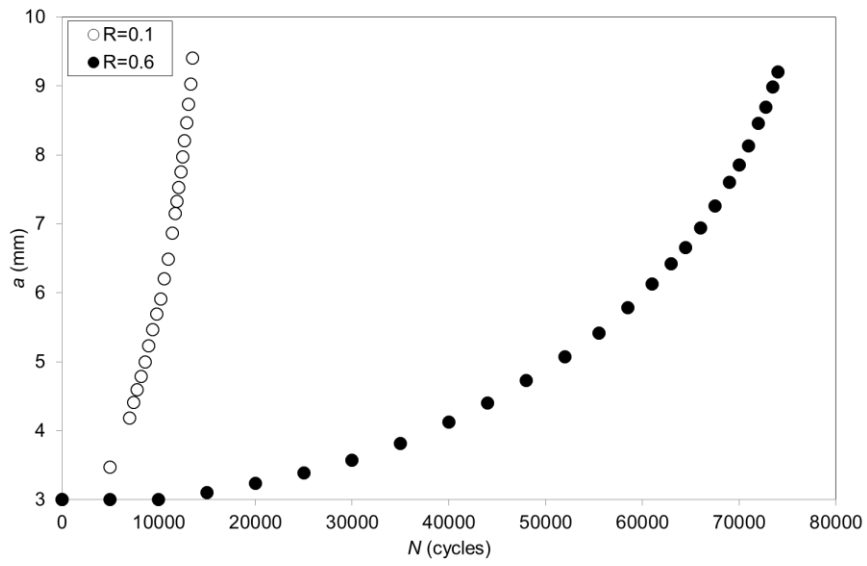
Figure 4   Crack length as a function of number of cycles for both specimens tested at stress ratios of 0.1 and 0.6.
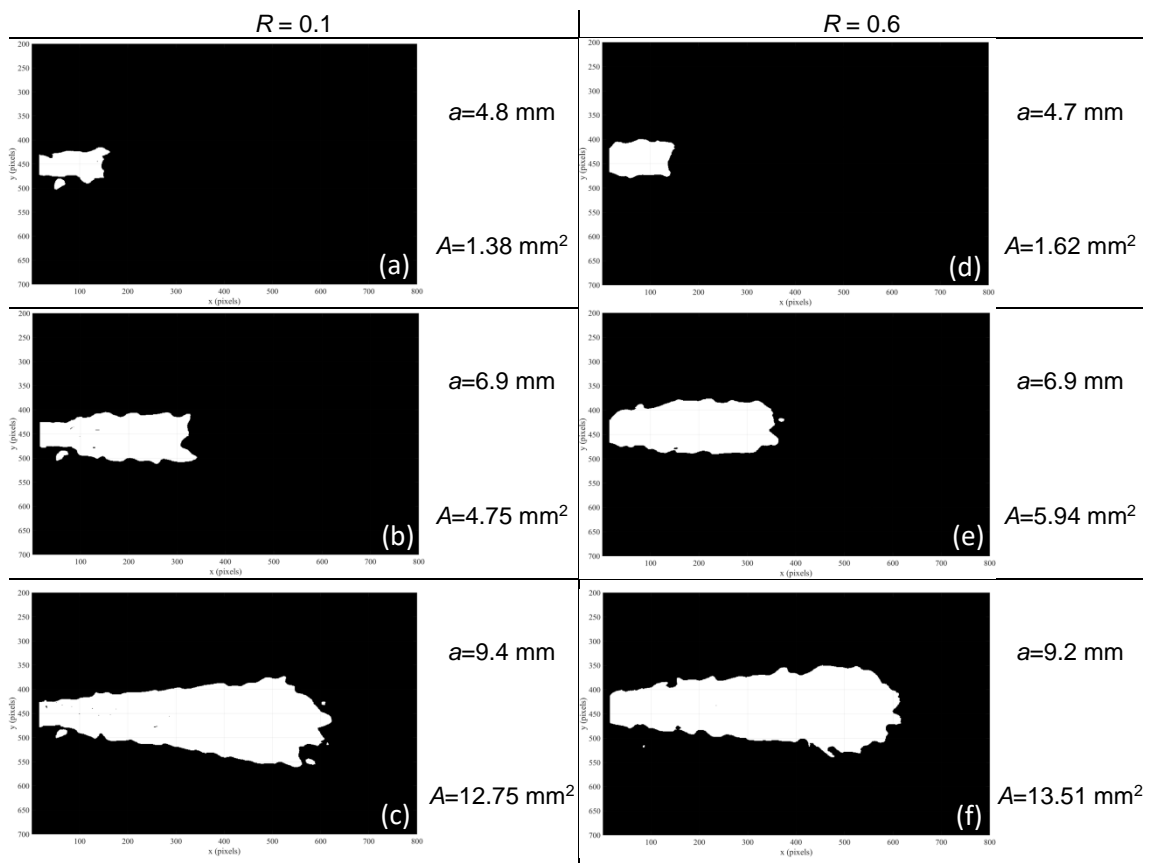
Figure 5   Extent of the plastic wake. Left column: data for R = 0.1 with crack lengths of (a) 4.8 mm, (b) 6.9 mm and (c) 9.4 mm long. Right column: data for R = 0.6 with crack lengths (d) 4.7 mm, (e) 6.9 mm and (f) 9.2 mm long.
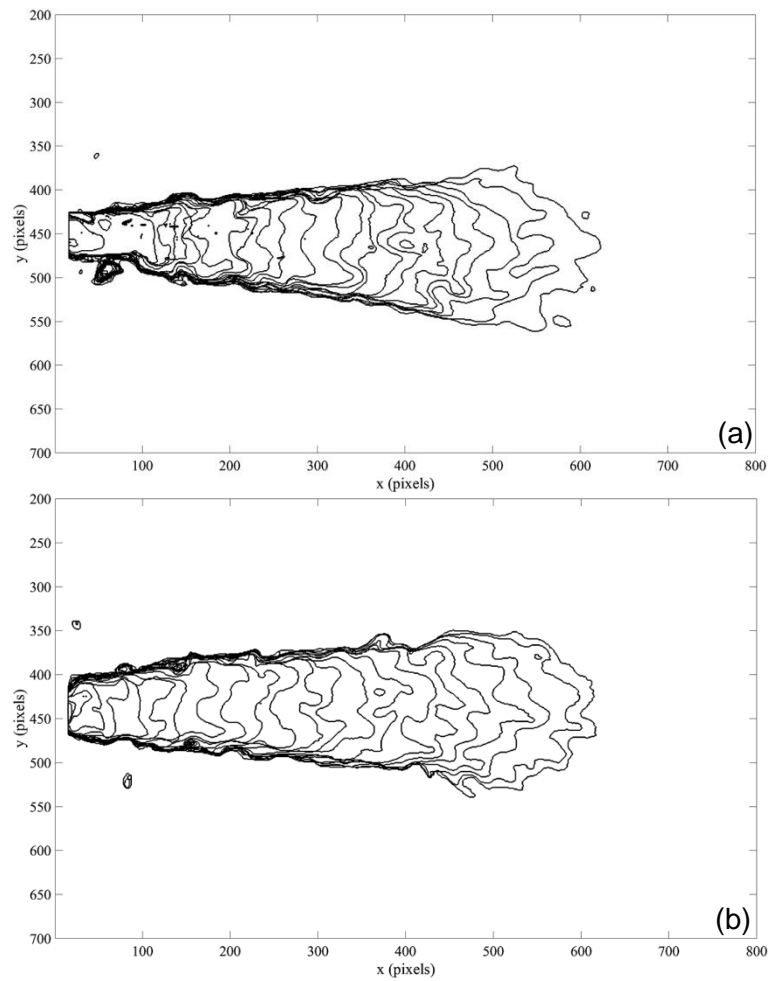
Figure 6   Development of the plastic wake as the crack grows for (a) R = 0.1 and (b) R = 0.6. The plastic wake contours shown, according to the data detailed in Table 3, are the following. R = 0.1: from datapoint 1 (5000 cycles, 3.5 mm crack) until datapoint 23 (13500 cycles, 9.4 mm crack); R = 0.6: from datapoint 5 (25000, 3.4 mm crack) until datapoint 25 (74000, 9.2 mm crack).
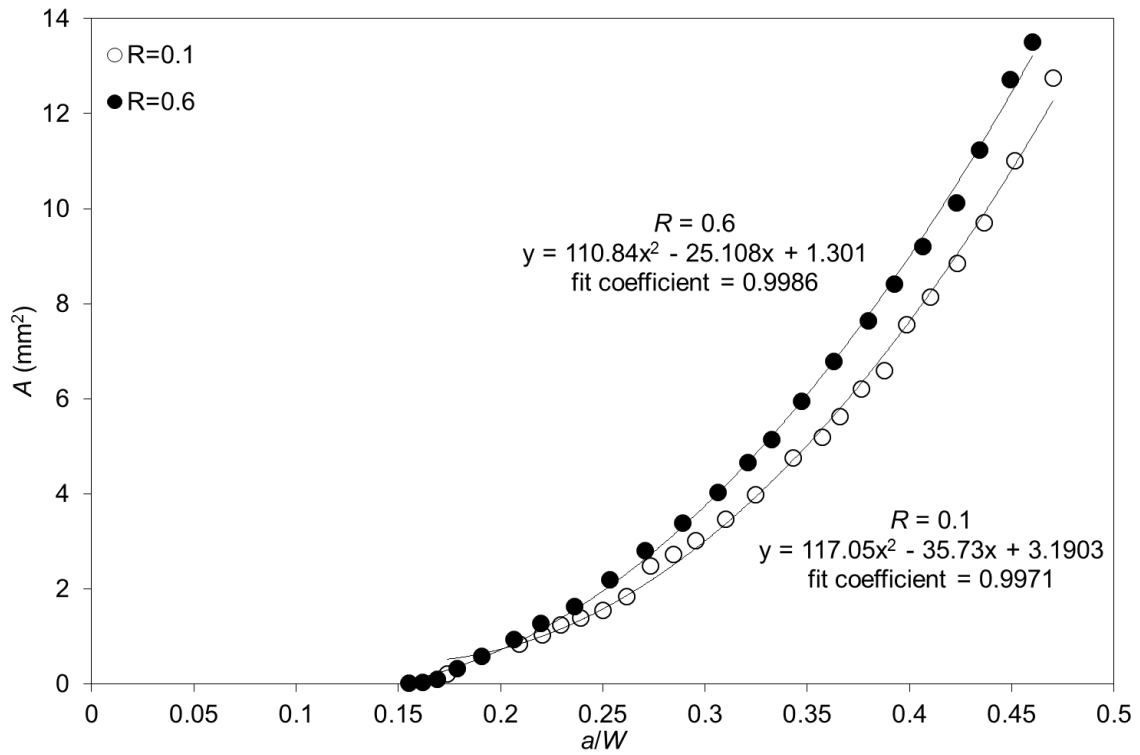
Figure 7   Evolution of the plastic wake area as a function of the normalised crack length for stress ratio values of 0.1 and 0.6.
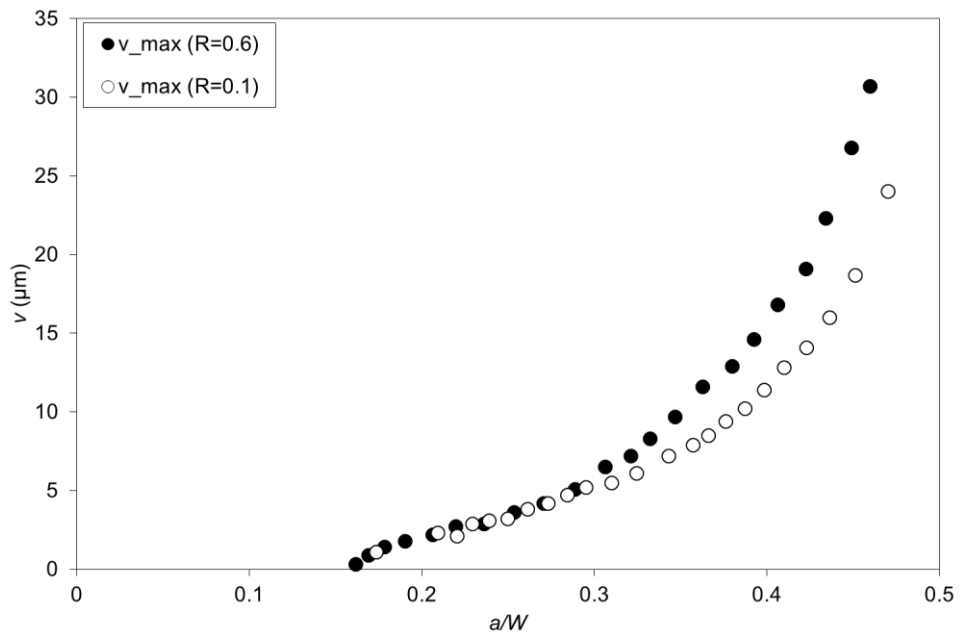
Figure 8   Maximum values of residual vertical displacements as a function of the normalised crack length for stress ratio values of 0.1 and 0.6.